analytical chemistry

Article

pubs.acs.org/ac

Multiscattering-Enhanced Absorption Spectroscopy

Volodymyr B. Koman, Christian Santschi,* and Olivier J. F. Martin

Nanophotonics and Metrology Laboratory (NAM), Swiss Federal Institute of Technology (EPFL), CH-1015 Lausanne, Switzerland

Supporting Information

ABSTRACT: An original scheme for sensitive absorption measurements, particularly well-suited for low analyte concentrations, is presented. The technique is based on multiscattering-enhanced absorption spectroscopy (MEAS) and benefits from the advantages of conventional absorption spectroscopy: simplicity, rapidity, and low costs. The technique relies on extending the optical path through the sensing volume by suspending dielectric beads in the solution containing the analytes of interest, resulting in multiple scattering of light, which increases the optical path length through the sample. This way, a higher sensitivity and lower limit of detection, compared to those of conventional absorption spectroscopy, can be achieved. The approach is versatile and can be used for a broad variety of analytes. Here, it is applied to the detection of phenol red, 10 nm gold nanoparticles, and envy green fluorescence dye; the limit of detection is decreased by a factor of 7.2 for phenol red and a factor of 3.3 for nanoparticles and dye. The versatility of this approach is illustrated by its application in increasing the sensitivity of colorimetric detection with gold nanoparticle probes and a commercially available hydrogen peroxide bioassay. The influence of different parameters describing the scattering medium is investigated in detail experimentally and numerically, with very good agreement between the two. Those parameters can be effectively used to tailor the enhancement for specific applications and analytes.

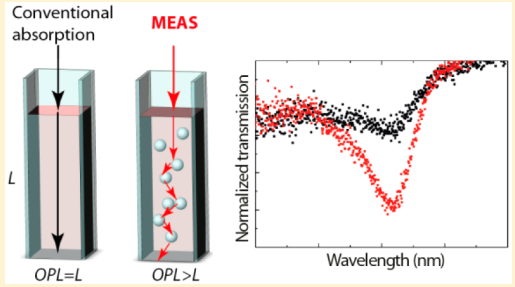

Absorption spectroscopy is a fast, simple, and inexpensive method for the detection of biomolecules such as nucleotides, proteins, steroids, antibiotics, amino acids, and terpenoids, as well as pharmaceuticals, pesticides, or hydrocarbons.[1−9] This diversity makes absorption spectroscopy a tool of choice for a broad range of applications in research, medical laboratories, and industry. Additionally, it complements separation techniques such as high-performance liquid chromatography[10] and capillary electrophoresis[11] to identify and quantify analytes. Recently, its field of applications has been broadened by novel assays, where molecules are tagged to quantum dots, nanoparticles, or fluorescent dyes to enhance assay performance.[12−15] Alternative methods for detecting biochemical entities such as mass spectroscopy[16] and electrochemistry[17] have their own limitations. Mass spectrometry requires extensive equipment, while in electrochemistry, the analyte must undergo a redox reaction, which limits the materials to which it can be applied. Further alternatives are chemoluminescence[18] and fluorescence.[19] However, these techniques can experience bleaching and require specific and often expensive optical filters and, furthermore, invasive chemical species that interact with the sample of interest. Because of all these limitations, absorption spectroscopy is a commonly used detection method.

In conventional absorption spectroscopy, the light beam passes through the absorbing sample and the spectral intensity of the light is measured before (I_0) and after the sample (I). If the absorption coefficient of the analyte under study is known, its concentration can be determined using Beer−Lambert's law:[20]

$$I = I_0 \exp(-\alpha C l) \quad (1)$$

where C is the molar concentration, l the optical path length of light, and α the molar absorption coefficient. The minimal detectable concentration is determined by the relative change of intensity $\Delta I/I_0 = (I_0 - I)/I_0$, which depends on the equipment used, the amount of averaging, etc. $\Delta I/I_0$ is typically limited for spectroscopic measurements to $\sim 10^{-4}$ or using specific data analysis algorithms to 5×10^{-6}, while smaller signals cannot be further distinguished from the background noise.[21,22] For many practical applications, the concentrations of the analyte provide intensity changes lying below the limit of detection (LOD). For example, a typical dye, rhodamine 6G, has the strongest absorption of 116000 cm^{-1} M^{-1} at the wavelength λ = 532 nm.[23] The detection of 0.1 nM rhodamine would require an optical path of 86 cm with a $\Delta I/I_0$ of $\sim 10^{-3}$ measurement accuracy.

The sensitivity of absorption spectroscopy can be improved by increasing the optical path of light (OPL), and several techniques have been developed to do so: photoacoustic spectroscopy,[24] thermal-lensing effects,[25] liquid-waveguide capillary cells,[26] cavity-enhanced spectroscopy,[27] integrating sphere,[28] and attenuated total reflection spectroscopy.[29] Unfortunately, all these techniques require rather expensive and sophisticated equipment, and a simple technique that can push the LOD below the limit of conventional absorption spectroscopy is of great

Received: June 20, 2014
Accepted: December 29, 2014
Published: December 29, 2014

DOI: 10.1021/ac502267q
Anal. Chem. 2015, 87, 1536−1543

interest. In the following, we show that disordered media, which increase the OPL via multiscattering, can significantly improve the LOD for absorption spectroscopy.

The phenomenon of multiscattering in disordered media has been extensively studied in the context of photon localization,[30−32] light harvesting for solar cells,[33] focusing light below the diffraction limit,[34] and gas cameras.[35] Additionally, we have recently reported some preliminary results with cross-linked proteins forming a multiscattering solid matrix.[36−38] In all these examples, disordered media have been purposefully introduced to improve photon localization or extend the optical path. Much work has been done for cases in which the disordered medium is an obstacle rather than an aid. For instance, sensing and imaging through tissues and distant galaxies gave rise to reflection spectroscopy and spatially offset spectroscopy techniques.[39−41]

The aim of this work is to provide a simple, tunable, and sensitive optical method, based on multiscattering in random media, for measuring low concentrations of dispersed or dissolved analytes. Examples of random media are thick membranes with a high filling factor used by Svensson et al.[35] Those membranes exhibit large OPLs and show an excellent performance for gas detection. However, similar porous membranes show an increased response time for measurements in liquids, because of the slow diffusion of the analyte.[42] Hence, diffusion of the analyte into the random media is a limiting factor for dynamic measurements performed in liquids. In the work presented here, the multiscattering configuration is achieved by introducing an appropriate density of dielectric spheres inside a solution containing the analyte of interest. In such a configuration, the diffusion is not an issue because active mixing can be performed, and consequently, a rapid diffusion of the analyte can be achieved. This multiscattering-enhanced absorption spectroscopy (MEAS) allows us to enhance the absorbance with respect to conventional absorption spectroscopy for a broad variety of analytes. Specifically, we demonstrate this technique for phenol red, 10 nm gold nanoparticles, and envy green fluorescence dyes. By applying MEAS to a hydrogen peroxide bioassay, we show that the sensitivity of the measurements can be increased and the optimal optical path length can be determined. To obtain a deeper understanding of the process, we also implement a model based on Monte Carlo calculations to simulate light propagation in disordered media.[43,44] This way, we show both experimentally and numerically that variations in size, concentration, and geometrical thickness of the scattering medium control the optical path enhancement. The possibility of OPL tuning provides a way to design disordered media adapted to the application at hand (limit of detection, diffusion, sensitivity, and robustness).

EXPERIMENTAL SECTION

Reagents. DMEM medium with phenol red (40 μM), 10 nm gold particles, and envy fluorescence dye encapsulated in 60 nm latex beads were purchased from Life Technologies (catalog no. 10566), BBI solutions (catalog no. EMGC10), and Bangs Laboratories (catalog no. FS02F), respectively. The polystyrene bead (PS) microsphere kit was purchased from Polysciences (catalog no. 19822-1), and the colorimetric assay for hydrogen peroxide detection was purchased from Cell BioLabs (OxiSelect, catalog no. STA-343). Because the DMEM medium without phenol red does not absorb in the visible range, in our experiments we attribute the absorption of the DMEM mixture with phenol red to the corresponding concentration of phenol red. In the following, when we mention "phenol red" dilutions, we refer to the dilution of pure phenol red, not to dilutions of the mixture DMEM with phenol red.

All dilutions are done with deionized water if not stated otherwise. Different PS bead diameters and concentrations are used to investigate the influence of multiscattering, as described in the text. It should be noted here that PS beads do not aggregate because of the presence of negatively charged surfactants (e.g., <0.1% sodium dodecyl sulfate, according to the supplier).

Optical Measurements. The spectral measurements are taken in transmission mode using a 20× objective (UPlanFL 20×, Olympus, NA = 0.41) and inverted microscope (IX71, Olympus) coupled to a monochromator (TRIAX 550, Horiba Scientific) and a liquid nitrogen-cooled CCD camera (Symphony, Horiba Scientific). The typical integration time to record one spectrum is on the order of 300 ms. The absorption spectra are normalized with reference spectra obtained by measuring the same solution without the absorbing element; i.e., pure water is used as the reference for conventional absorption spectroscopy, while water with dispersed PS beads is used as the reference for MEAS. It must be mentioned that not the entire spectrum but only the values at the absorption peaks are used as reference points: λ = 520 nm for gold nanoparticles, λ = 530 nm for envy green dye, λ = 570 nm for phenol red, and λ = 595 nm for H_2O_2 bioassays. Standard 384-well plates containing cuvettes with a 3.3 mm × 3.3 mm square cross section are used as the sample chamber, except for the experiments with varying thicknesses, where 96-well plates with a 7.3 mm × 7.3 mm cross section are used. This precaution prevents cross-talk between neighboring cells. For 40 μL samples, we did not observe cross-talk in 384-well plates, but experiments with a 1 cm optical path require a 96-well plate with a larger cross section to effectively suppress cross-talk. Using such wells demands only small volumes of analyte, which is advantageous for expensive biological samples. However, MEAS can also be implemented in larger absorption spectroscopy cuvettes.

RESULTS AND DISCUSSION

When light passes through the cuvette containing a homogeneous solution, its optical path is determined by the geometrical thickness L of the sample. In the following, absorption enhancement refers to a configuration corresponding to standard absorption spectroscopy. If the sample is inhomogeneous, i.e., exhibits noticeable spatial variations of the refractive index, the passing light undergoes multiscattering. Consequently, the OPL is increased as schematically illustrated in Figure 1. In this work, this is achieved by adding spherical PS particles to the solution containing the analyte. Hence, the OPL becomes longer than the geometrical thickness of the sample, resulting in multiscattering-enhanced absorption spectroscopy.

Let us first illustrate this approach by measuring the transmission through a cuvette containing 40 μL of a 0.6 μM phenol red solution diluted in water, corresponding to a geometrical thickness L of 3.7 mm. The baseline is determined by transmission measurements trough the cuvette containing the same volume of pure water. In the second cuvette, we prepared a mixture containing 0.6 μM phenol red and 0.6 nM PS beads with a diameter d of 0.5 μm. To determine the baseline for this configuration we record the transmission spectrum of a 40 μL dispersion containing the same concentration of PS beads in pure water. We obtain two normalized transmission spectra for the same phenol red solution concentration. As sketched in Figure 1, the absorption dip of phenol red is much less pronounced in the absorption spectroscopy measurement than in the MEAS

DOI: 10.1021/ac502267q
Anal. Chem. 2015, 87, 1536−1543

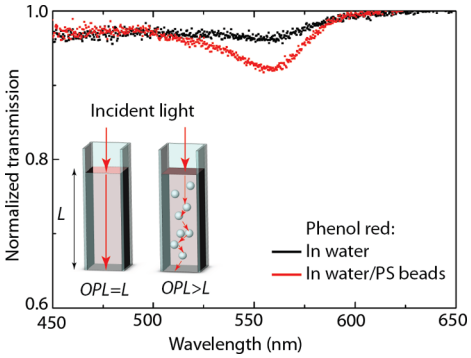

Figure 1. Normalized transmission measurements for the two configurations: 0.6 μM phenol red in water and 0.6 μM phenol red with 0.6 nM PS beads (d = 0.5 μm) in water. The inset shows a schematic drawing of the absorption spectroscopy and the MEAS configurations. The optical path length (OPL) is increased by the presence of the scatterers in the MEAS configuration.

configuration, which clearly indicates in the latter case an enhanced absorption due to multiscattering.

Improving the Limit of Detection by MEAS. We now quantify the enhancement provided by MEAS and compare the performance of this technique with that of conventional absorption spectroscopy for three different analytes: phenol red, 10 nm gold nanoparticles, and envy green fluorescence dye. Phenol red is commonly used in colorimetric measurements to determine the pH of a solution, because the magnitude of its absorption dip at λ = 570 nm is sensitive to pH.[45] Following the same experimental procedure as described above for Figure 1, we measure the unitless absorbance A for different phenol red concentrations, using eq 2:

$$A = -\ln\left(\frac{I}{I_0}\right) = \alpha C l \tag{2}$$

where I and I_0 are the measured intensities of the outcoming light and the baseline, respectively. The measurements are carried out using water and two mixtures containing 0.5 μm PS beads at two different concentrations: $C^{ps}{}_1$ = 0.6 nM, and $C^{ps}{}_2$ = 3.0 nM. Figure 2A shows that the absorbance A is proportional to phenol red concentration, which is in agreement with Beer–Lambert's law. To quantify the enhancement of the absorbance, we introduce a factor k defined as the ratio between the absorbance of the analyte in water and in the water/PS bead dispersion for a given wavelength:

$$k = A_{\text{in water/PS}}/A_{\text{in water}} \tag{3}$$

Compared to that of the solution without polystyrene beads, the presence of PS beads increases the absorbance A by a factor k_1 of 3.3 for $C^{ps}{}_1$ and a factor k_2 of 7.2 for $C^{ps}{}_2$. The horizontal line in Figure 2A corresponds to 3 times the noise level. Its intersection with the absorbance of the solution gives the calculated LOD, which scales linearly with the inverse of k. Defining LOD_{PS} as the limit of detection in the solution with dispersed PS beads and LOD as the limit of detection without them, we obtain

$$\text{LOD}_{\text{PS}} = \text{LOD}/k \tag{4}$$

Therefore, MEAS significantly reduces the LOD of phenol red from 200 to 28 nM. The amplification factor k does not depend on phenol red concentration C, and according to eq 2, the OPL scales linearly with k:

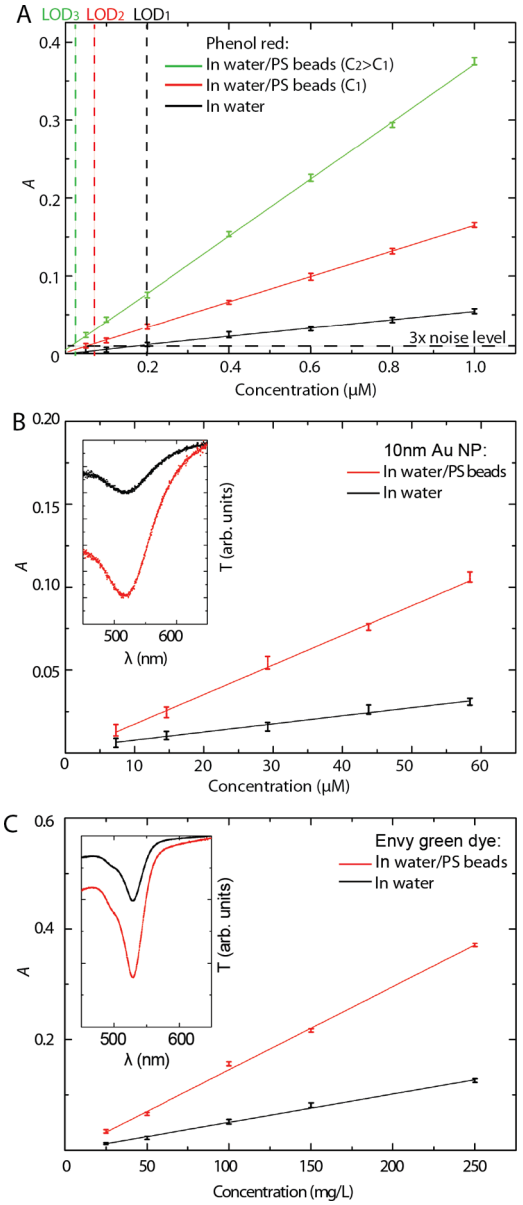

Figure 2. Absorption enhancement for different analytes. (A) Phenol red absorbance A in water only and in water with two different concentrations of PS beads (0.5 μm) ($C^{ps}{}_1$ = 0.6 nM, and $C^{ps}{}_2$ = 3.0 nM); 3 times the noise level determines the LOD at λ = 570 nm. (B) Absorbance A for 10 nm Au nanoparticles in water and in water/PS beads (d = 0.5 μm; $C^{ps}{}_1$) at λ = 520 nm. The inset shows the normalized transmission spectrum T of the nanoparticles. (C) Same as panel B for envy green fluorescence dye at λ = 530 nm. The error bars represent the standard deviation over five measurements.

$$\text{OPL}_{\text{PS}} = k \times \text{OPL} \tag{5}$$

where OPL_{PS} refers to the bead configuration and OPL to the optical path length without PS beads. While absorption spectroscopy is routinely used for colorimetric measurements, other assays use tagging strategies in which the molecule of interest is attached to various types of quantum dots, nanoparticles, or fluorescent dyes that enhance the performance of such assays and serve as indicators of the presence of molecules. MEAS can also be utilized in that context, and in the following, we demonstrate its utilization for the detection of gold nanoparticles or fluorescent dyes. The scattering of >100 nm

DOI: 10.1021/ac502267q
Anal. Chem. 2015, 87, 1536–1543

gold nanoparticles dominates their absorption, and such nanoparticles can be detected with high sensitivity using a dark-field configuration.[46,47] This is not the case for nanoparticles <55 nm in diameter, for which the scattering cross section drops dramatically and the absorption cross section starts to dominate.[46,48] However, the latter remains very weak for such small gold nanoparticles, which makes their detection quite challenging, so that only a few complicated techniques have been successfully demonstrated so far.[49−51] This is detrimental for novel nanodevices that rely on extremely small metallic nanoparticles.[52,53] Similarly, fluorescent dyes are the basis for a large number of assays commonly used in biology and chemistry, and the ability to measure their absorption can provide additional quantitative information.[54] Applying the same experimental scheme, we measure the transmission for 10 nm gold nanoparticles and envy green fluorescence dyes dissolved in water or in a water/PS bead (d = 0.5 μm) dispersion with a bead concentration (C^{ps}) of 0.6 nM. The corresponding absorbences A are shown in panels B and C of Figure 2. The 10 nm gold nanoparticles have an absorption dip at λ = 520 nm, while the envy green fluorescence dye absorbs at λ = 530 nm. Note that it is quite exceptional to be able to measure the signal of nanoparticles as small as 10 nm. As for the phenol red, absorbance A is proportional to concentration C of the solution. When the scattering medium is used, an enhancement factor (k) of 3.3 is observed for both the nanoparticles and the dye, while the LOD decreases correspondingly. These results suggest that enhancement factor k does not depend on the type of analyte but changes only with C^{ps}, as will be investigated below.

Enhancing the Sensitivity of Bioassays by MEAS. In addition to the LOD, sensitivity S represents an important parameter for bioassays. This parameter is of special interest when the analyte evolves with time (i.e., changes its absorption α or its concentration C), for instance, during a chemical reaction or a biological process. In absorption spectroscopy, the sensitivity describes how the transmitted light intensity changes:

$$S = \left|\frac{\partial}{\partial C}\frac{\Delta I}{I_0}\right| + \left|\frac{\partial}{\partial \alpha}\frac{\Delta I}{I_0}\right| \tag{6}$$

Here we restrict ourselves to the case in which the intensity changes only with concentration, thus:

$$S = \left|\frac{\partial}{\partial C}\frac{\Delta I}{I_0}\right| = \alpha l e^{-\alpha C l} \tag{7}$$

From eq 7, we see that in a fixed volume with a given α and C the sensitivity cannot be changed in conventional absorption spectroscopy. In contrast, S can be tuned by changing the OPL in MEAS (Figure 3A). For a short l, S is very small because the system is in the weak-absorbing regime (regime I in Figure 3A) and large changes in C are needed. On the other hand, when l is very large, the medium absorbs most of the light and S drops also toward low sensitivity (regime III in Figure 3A). The optimal OPL l_{opt} for which the sensitivity reaches its maximum is where $\partial S/\partial l$ = 0, leading to eq 8 (regime II in Figure 3A):

$$l_{opt} = \frac{1}{\alpha C} \tag{8}$$

For a given α and C, with the corresponding l_{opt} given by eq 8, the maximal sensitivity is $S_{opt} = e^{-1}/C$. To demonstrate this experimentally, we show that the sensitivity and LOD of a commercially available assay for the detection of hydrogen peroxide (OxiSelect) can be improved for low concentrations. It is worth noting here that H_2O_2 plays an important role in biological systems: it acts as a signaling molecule in a broad variety of transduction processes and is a marker for oxidative stress, which is involved in aging but also in various diseases.[55,56] The principle of the bioassay lies in the oxidation of Fe^{2+} to Fe^{3+} in the presence of H_2O_2, which forms a ferric xylenol orange (Fe-XO) complex. The formation of Fe-OX complexes leads to an alteration of the molar absorption coefficient, providing information about the H_2O_2 concentration present in the solution. The experiments described herein are conducted using the bioassay according to the instructions provided by the supplier; in particular, the absorption is determined at λ = 595 nm. Not only the H_2O_2 concentration but also the rate of change is a very important parameter when studying biological processes. The sensitivity for different H_2O_2 concentrations is determined by measuring the change in the signal when 1 μM H_2O_2 is added to a known concentration. Similarly, we measure the sensitivity S^{PS} in the presence of 0.6 nM PS beads having a diameter of 0.5 μm. As observed in the previous experiments, the OPL increases by a factor k of 3.3 for an L of 3.7 mm, and consequently, S^{PS} is enhanced for low concentrations as shown in Figure 3B. Moreover, the lower limit of the working range, given as 1 μM by the manufacturer, can be reduced to 300 nM. In the configuration at hand, S^{PS} is larger than S in water for H_2O_2 concentrations smaller than the threshold value (C_{th} = 30 μM), while for higher concentrations, sensitivity S without PS beads

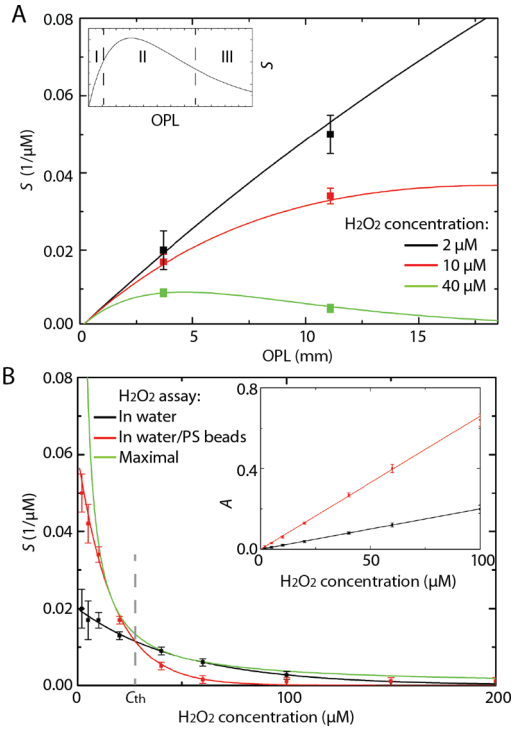

Figure 3. Sensitivity S of the H_2O_2 assay (A) as a function of OPL for a fixed concentration and (B) as a function of concentration, in an L = 3.7 mm cuvette filled with water and a 0.6 nM PS bead dispersion (d = 0.5 μm; k = 3.3) at λ = 595 nm. Points refer to measurements, and lines are fit according to eq 7. The OPL is calculated using eq 5. The inset in panel A shows three distinct regions: (I) growing sensitivity, (II) maximal sensitivity, and (III) decreasing sensitivity. The inset in panel B shows absorbance A in water and in a water/PS bead dispersion (d = 0.5 μm) (C^{ps} = 0.6 nM; L = 3.7 mm; k = 3.3). The error bars represent the standard deviation over five measurements.

DOI: 10.1021/ac502267q
Anal. Chem. 2015, 87, 1536−1543

dominates. The expressions for S_{opt} and l_{opt} suggest that very high sensitivities can be achieved for low concentrations with a corresponding large l_{opt} (eq 8). In our experiments, we show that we are able to improve the performance of the bioassay by the factor $S^{PS}/S = 2.5$ for 2 μM H_2O_2. Therefore, the concentration of the PS beads can be adapted to obtain the maximal sensitivity for the concentration range of interest.

Enhancing the Sensitivity of Colorimetric Detection with Gold Nanoparticle Probes. For a further demonstration of the performance of MEAS, we study the aggregation of 10 nm gold nanoparticles in the presence of hexanedithiol. Dispersed gold nanoparticles can be used as basis for sensitive colorimetric probes.[57] In this experiment, the two free thiol groups of hexanedithiol can bind two or more gold nanoparticles together. This leads to a gradual aggregation of the nanoparticles, which can be monitored via the optical response. As shown earlier, 10 nm gold nanoparticles exhibit an absorption peak at λ = 520 nm that decreases with progressive aggregation of the nanoparticles (Figure 4). At the same time, a broad peak corresponding to the

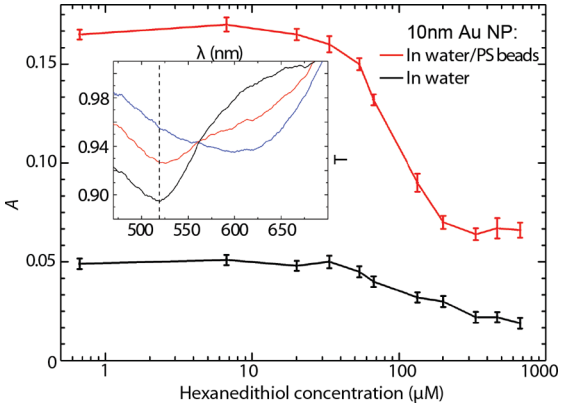

Figure 4. Absorbance A of 10 nm gold nanoparticles (80 μM) with respect to different concentrations of hexanedithiol in water and in a water/PS bead dispersion (d = 0.5 μm; C^{ps} = 0.6 nM; L = 3.7 mm; k = 3.3). The error bars represent the standard deviation over five measurements. The inset shows examples of normalized transmission T spectra for concentrations of 20 μM (black), 134 μM (red), and 670 μM (dark blue). The dashed line indicates the wavelenegth (λ = 520 nm) at which A was calculated.

aggregated particles emerges at higher wavelengths. Thus, A can be directly related to the amount of hexanedithiol in the solution. If the described experimental scheme is applied in water, A decreases from 0.05 to 0.02 upon addition of hexanedithiol. In contrast, in a water/PS bead dispersion with a bead concentration C^{ps} of 0.6 nM, A changes from 0.16 to 0.07, indicating an enhancement k of 3.3. It is worth mentioning that hexanedithiol does not bind to the PS bead surface. In conclusion, we demonstrate an enhanced sensitivity to hexanedithiol using 10 nm gold nanoparticles as colorimetric probes in MEAS, compared to conventional absorption spectroscopy.

Monte Carlo Calculations. Scattering of light in random media is a complex phenomenon, especially when the size of the scatterer is comparable to the wavelength of the light, as is the case in our configuration. The scattering for an individual particle in such a system is shown in Figure 5A. The total scattering cross section of the system results from the superposition of the individual amplitudes, making the problem rather complicated. Transport theory[58−60] and probabilistic Monte Carlo simulations[43,61] are the two main numerical methods used to tackle this problem. While the former method requires the knowledge of the macroscopic parameters of the system such as density and diffusion coefficient, the latter resorts to microscopic parameters such as the distance between the particles and their size. Here we use the Monte Carlo procedure to gain a better understanding of the multiscattering phenomenon and to study the influence of the various parameters describing the PS bead dispersion in the absorbing medium.

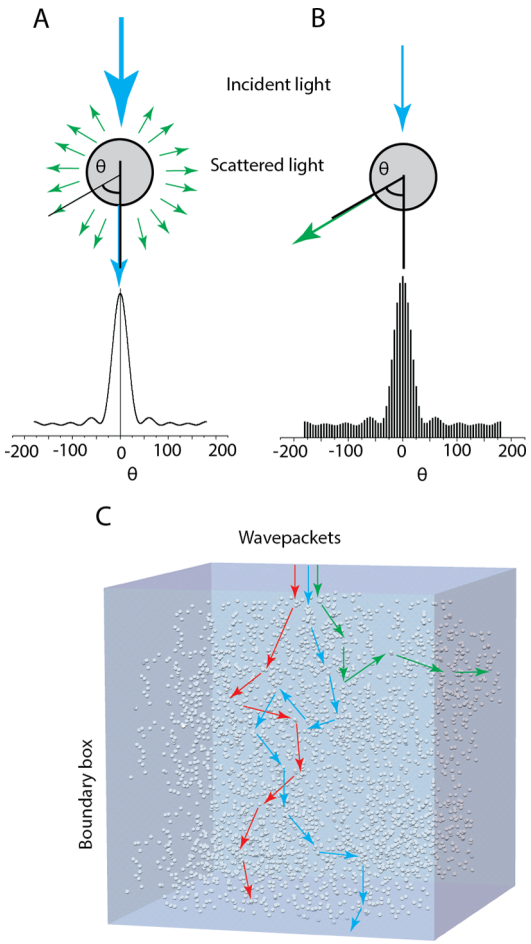

Figure 5. (A) Schematic illustration of the Mie scattering process. The incident light is scattered by the particle in all directions. The graph shows the scattering angle θ distribution. (B) Simulated scattering process. The incident light is scattered probabilistically in one direction, following Mie theory. A collection of wavepackets leads to the probability distribution shown in the graph, which agrees well with the Mie scattering distribution in panel A. (C) Schematic drawing of three wavepackets propagating through a box with a random scattering medium.

The scattering process is simulated as follows. We make use of the linearity of scattering intensity and divide the incident light into wavepackets that are sequentially launched into the system. Wavepackets have been chosen instead of single photons to simulate the absorption along the OPL. To describe each scattering event between wavepackets and particles, we introduce a probability function that describes the angular dependence of the scattering. This function depends on scattering cross section σ of the particle and is approximated by the Henyey−Greenstein distribution.[62] The wavepacket continues to propagate after the scattering event in a randomly chosen direction determined using the probability function that reproduces the angular

DOI: 10.1021/ac502267q
Anal. Chem. 2015, 87, 1536−1543

dependence of the scattering (Figure 5B). Thus, scattering from a large ensemble of wavepackets resembles a realistic scattering distribution. Because PS bead absorption is very weak and, moreover, is canceled out by the appropriate baseline in the experiment, it can be neglected in the simulations. Hence, only absorption from the background medium between two successive scattering events is considered.

This probabilistic Monte Carlo approach is implemented using MATLAB. First, we define the geometry, i.e., a box with dimensions identical to those used in the experiments, containing the random medium (Figure 5C). To achieve a reasonable approximation of a realistic system, 10^8 wavepackets representing the incident unpolarized light are launched at the central point of the top surface of the box. For each incident wavepacket, the intensity is assumed to be unity. The mean free path of light (l_{free}) between the scattering events is determined by the PS bead concentration (C^{PS}), the scattering cross section (σ), and the size (d) of the introduced beads as described below. The value of σ for the beads is calculated using Mie theory.[44] The attenuation of the wavepacket intensity between successive scattering events is calculated according to Beer's law (eq 1). All wavepackets escaping from the bottom surface of the box into a cone corresponding to the numerical aperture used in the experiment (NA = 0.41) are registered. The refractive indices for PS (n_{PS}) and the surrounding medium (water) (n_{H_2O}) are 1.6 and 1.33, respectively. The simulations have been conducted at the absorption peak wavelength (λ_d) of the solution of interest (e.g., λ_d = 570 nm for phenol red). For the calculations, we assume a random distribution of the PS beads, characterized by the random distance between particles: $p = -l_{free} \log \Sigma$, where Σ is a random number between 0 and 1.[43]

Note that this approach does not hold for densely packed or so-called short-range random media.[63] In that case, densely packed scatterers modify the refractive index of their neighbors and influence the Mie scattering properties of each particle. The short-range regime is reached when l_{free} becomes smaller than the diameter d of the scatterer. We consider that low scatterer concentrations correspond to $l_{free} \gg d$, whereas moderate concentrations are characterized by $l_{free} \gtrsim d$. Here, we are clearly working in the former regime because l_{free} ranges from 5 to 25 μm compared to d = 0.5 μm, and the model can be applied. On the other hand, l_{free} is much smaller than geometrical thickness L, which fulfills the condition that wavepackets propagating in such a medium experience multiscattering.

Control of the OPL Enhancement. Let us now use the model described in the previous section to discuss the parameters that influence the OPL in a random medium. The enhancement of the OPL is determined by the number of times the wavepackets are scattered while traveling through the disordered medium. For a multiscattering medium, the OPL scales with the reciprocal value of the mean free path (l_{free}) in the dispersion:[64]

$$\mathrm{OPL} \sim \frac{1}{l_{free}} \tag{9}$$

The mean free path in the dispersion can be determined using[65,66]

$$l_{free} = \frac{2d}{3FQ_{sca}(1-g)} \tag{10}$$

where F ($=\pi d^3 C^{PS}/6$) is the filling factor, Q_{sca} is the scattering efficiency for each individual scatterer, and g ($=\langle \cos\theta \rangle$) is the average scattering angle. We consider only nonopaque samples because low absorption measurements are of special interest for absorption spectroscopy.

As seen from the experiments with phenol red (Figure 2A), the PS bead concentration, and thus filling factor F, affects the OPL enhancement.[67] If C^{PS} is low, l_{free} becomes larger than L; hence, k goes to unity, and the system is no longer in the multiscattering regime. Figure 6A displays both measured and simulated k values as a function of F for phenol red. The graph indicates that k can be increased to 15 for F = 0.1. It is worth mentioning that the value of F has an upper limit that is determined by the closely packed configuration; i.e., F cannot go beyond 0.5−0.7 depending on the type of packing.[68] Note in Figure 6A the excellent agreement between simulations and measurements.

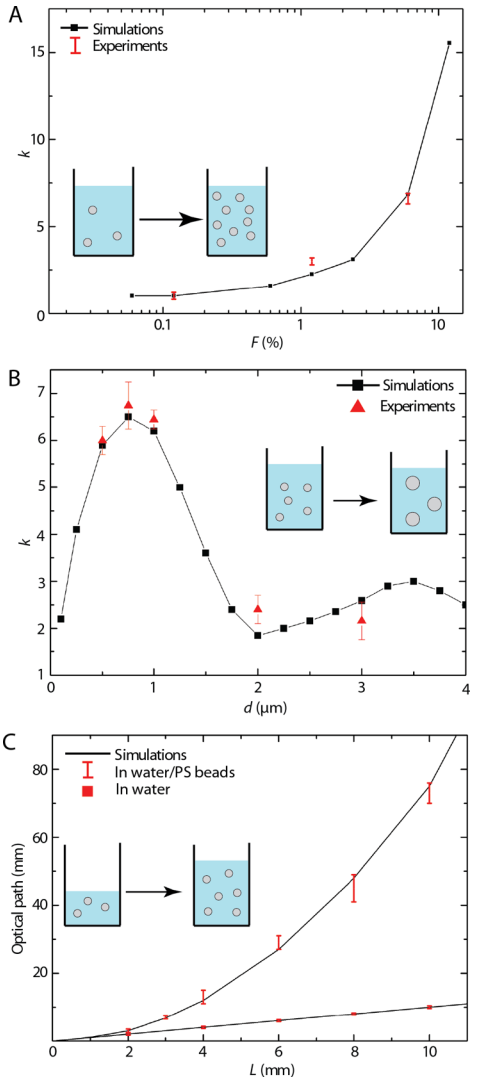

Figure 6. (A) Optical path length (OPL) enhancement as a function of PS bead filling factor F for a 40 μL mixture, when changing the concentration of the PS beads (d = 0.5 μm). (B) OPL enhancement for PS beads with different sizes for a 40 μL mixture, keeping filling factor F equal to 0.052. (C) Optical path for phenol red in water and in a water/PS bead dispersion (d = 0.5 μm) (calculated using eq 5) as a function of measurement cell thickness L. The PS bead concentration (C^{ps}) is kept constant at 0.6 nM. Error bars represent the standard deviation for five samples.

It should be emphasized that the numerical analysis of MEAS relies on a homogeneous statistical distribution of the scatterers

DOI: 10.1021/ac502267q
Anal. Chem. 2015, 87, 1536−1543

within the sample volume. Hence, aggregation of the scatterers can reduce the OPL enhancement. Such an aggregation is more likely for a high PS bead concentration. Aggregation can be caused by the background media, which could reduce the OPL enhancement and hence the sensitivity. More detrimental is the case in which aggregation is caused by the analyte itself, because in that case the baseline measurement corresponds to a nonaggregated system. However, in our experiments, we are targeting very low concentrations of analytes, which limits aggregation. It goes without saying that the scattering medium should not interfere chemically with the species under study; this is the case for the PS beads used in the different experiments reported here.

To investigate the influence of the PS bead size, we prepare bead dispersions with different concentrations (C^{PS}) and different diameters (d) while keeping the filling factor (F) constant; the following PS bead diameters and concentrations are used: 0.5 μm and 3.0 nM, 0.75 μm and 0.9 nM, 1 μm and 0.375 nM, 2 μm and 38 pM, and 3 μm and 14 pM, respectively. Because 2 and 3 μm beads sediment in water within a few minutes, the solution density must be increased by addition of 0.05 g/mL glucose leading to a final density of 1.02 g/mL, which efficiently hinders sedimentation (PS density ρ = 1.05 g/mL; glucose ρ = 1.6 g/cm^3). This addition of glucose does not significantly affect the refractive index of the solution, which changes from 1.33 to 1.34. In this case, eq 10 leads to OPL $\sim Q_{sca}g/d$. We compare k for a 40 μL solution with that for a 1 μM phenol red solution (Figure 6B). A maximum of the k value can be observed for PS beads with a diameter d of 0.75 μm. Simple calculations using Mie theory show that Q_{sca} strongly varies with d while the change in the value of g is insignificant. Furthermore, the two maxima of the k values around d = 0.75 and 3.5 μm agree well with maxima in Q_{sca} obtained from Mie theory. It is worth mentioning that Q_{sca} can also be tailored by tuning refractive index contrast Δn between the surrounding medium and the particle.[69]

It is known that for disordered media the OPL increases with L^2 as the number of scattering events also increases with L.[35] Consequently, according to eq 5, enhancement factor k increases with L, and therefore, MEAS, compared to absorption spectroscopy, benefits even more from increasing L. To vary geometrical thickness L, we prepare a solution of 1 μM phenol red with 0.6 nM PS beads (d = 0.5 μm) and add different volumes of the mixture to a 96-well plate (the larger cross section available in such a well ensures no cross-talk between neighboring wells). Transmission measurements confirm that the OPL of phenol red in water increases linearly with L (Figure 6C), whereas in a water/PS bead dispersion, it grows quadratically with L. For conventional absorption spectroscopy, L changes from 4 to 10 mm, whereas for MEAS, an increase from 13.2 to 73 mm is observed in Figure 6C, corresponding to a change in absorption enhancement k from 3.3 to 7.3.

Spectral Dependence of the OPL Enhancement. Until now, we have determined k for only a single wavelength. As follows from eqs 9 and 10, k changes with wavelength because of the dispersive nature of Q_{sca} (while g also contributes to this effect, its dispersion is much weaker than that of Q_{sca}).[69] As indicated in the Supporting Information, for the experiments with phenol red, gold nanoparticles, and envy green reported here, k changes by only 2% in the wavelength range of 450−650 nm [d = 0.5 μm; F = 0.0104; L = 4 mm (see Figures S5 and S6 of the Supporting Information)], with the largest value of k obtained for the smallest wavelength, in good agreement with Rayleigh scattering.[69] The dispersion increases further with cell thickness L, filling factor F, or PS bead diameter d (Figures S7 and S8 of the Supporting Information). Finally, the relation $k \sim L$ remains valid over the whole spectrum (Figure S9 of the Supporting Information).

CONCLUSIONS

We have presented a new scheme for sensitive absorption measurements, particularly well-suited for low analyte concentrations. The technique is based on multiscattering-enhanced absorption spectroscopy (MEAS). Like conventional absorption spectroscopy, MEAS is fast, simple, and inexpensive. After the introduction of PS beads into a solution containing the analyte, light undergoes multiscattering, which increases the optical path length through the sample. This way, a higher sensitivity and lower LOD, compared to those of conventional absorption spectroscopy, can be achieved. The approach is versatile and can be used for a broad variety of analytes. Here, it has been applied to the detection of phenol red, 10 nm gold nanoparticles, and envy green fluorescence dye, and we have observed that the LOD is decreased by a factor of 7.2 for phenol red and a factor of 3.3 for nanoparticles and dye. Furthermore, the sensitivity and working range of a commercially available hydrogen peroxide bioassay have been improved by almost 1 order of magnitude, which convincingly demonstrates the versatility of the technique. The influence of the concentration and size of PS beads as well as geometrical thickness L of the sample on the OPL in the disordered medium has been investigated numerically and experimentally. Those parameters can be effectively used to tailor the enhancement for specific applications and analytes. The results of performed experiments are in excellent agreement with numerical simulations based on a probabilistic approach.

ASSOCIATED CONTENT

Supporting Information

Detailed measured spectra for phenol red, gold nanoparticles, and envy green and a H_2O_2 bioassay. This material is available free of charge via the Internet at http://pubs.acs.org.

AUTHOR INFORMATION

Corresponding Author

*E-mail: christian.santschi@epfl.ch.

Notes

The authors declare no competing financial interest.

ACKNOWLEDGMENTS

This work was supported by the Swiss National Science Foundation in the framework of Swiss National Research Program NRP 64 Project 406440-131280/1.

REFERENCES

(1) Pradier, C.-M.; Salmain, M.; Zheng, L.; Jaouen, G. *Surf. Sci.* **2002**, *502−503*, 193−202.
(2) Zubavichus, Y.; Shaporenko, A.; Korolkov, V.; Grunze, M.; Zharnikov, M. *J. Phys. Chem. B* **2008**, *112*, 13711−13716.
(3) Roe, A. L.; Schneider, D. J.; Mayer, R. J.; Pyrz, J. W.; Widom, J.; Que, L. *J. Am. Chem. Soc.* **1984**, *106*, 1676−1681.
(4) Namjou, K.; Roller, C. B.; Reich, T. E.; Jeffers, J. D.; McMillen, G. L.; McCann, P. J.; Camp, M. A. *Appl. Phys. B: Lasers Opt.* **2006**, *85*, 427−435.
(5) Shervani, Z.; Etori, H.; Taga, K.; Yoshida, T.; Okabayashi, H. *Colloids Surf., B* **1996**, *7*, 31−38.

DOI: 10.1021/ac502267q
Anal. Chem. 2015, 87, 1536−1543

(6) Kaznacheyev, K.; Osanna, A.; Jacobsen, C.; Plashkevych, O.; Vahtras, O.; Ågren, H.; Carravetta, V.; Hitchcock, A. P. *J. Phys. Chem. A* **2002**, *106*, 3153−3168.
(7) Maris, E. P.; Ketchie, W. C.; Oleshko, V.; Davis, R. J. *J. Phys. Chem. B* **2006**, *110*, 7869−7876.
(8) Wang, T.; Walden, S.; Egan, R. *J. Pharm. Biomed. Anal.* **1997**, *15*, 593−599.
(9) Anawar, H.; Garcia-Sanchez, A.; Hossain, M.; Akter, S. *Bull. Environ. Contam. Toxicol.* **2012**, *89*, 620−625.
(10) Riley, C. M.; Sternson, L. A.; Repta, A. J. *Anal. Biochem.* **1982**, *124*, 167−179.
(11) Li, R.; Loock, H.-P.; Oleschuk, R. D. *Anal. Chem.* **2006**, *78*, 5685−5692.
(12) Chen, W.-Y.; Chen, L.-Y.; Ou, C.-M.; Huang, C.-C.; Wei, S.-C.; Chang, H.-T. *Anal. Chem.* **2013**, *85*, 8834−8840.
(13) Dou, Y.; Yang, X.; Liu, Z.; Zhu, S. *Colloids Surf., A* **2013**, *423*, 20−26.
(14) Tong, S.; Ren, B.; Zheng, Z.; Shen, H.; Bao, G. *ACS Nano* **2013**, *7*, 5142−5150.
(15) Zhang, Y.; Pilapong, C.; Guo, Y.; Ling, Z.; Cespedes, O.; Quirke, P.; Zhou, D. *Anal. Chem.* **2013**, *85*, 9238−9244.
(16) Shevchenko, A.; Wilm, M.; Vorm, O.; Mann, M. *Anal. Chem.* **1996**, *68*, 850−858.
(17) Armstrong, F. A.; Hill, H. A. O.; Walton, N. J. *Acc. Chem. Res.* **1988**, *21*, 407−413.
(18) Rauhut, M. M. *Acc. Chem. Res.* **1969**, *2*, 80−87.
(19) Valeur, B.; Berberan-Santos, M. N. *J. Chem. Educ.* **2011**, *88*, 731−738.
(20) Bohren, C. F.; Huffman, D. R. In *Absorption and Scattering of Light by Small Particles*; Wiley-VCH Verlag GmbH: Berlin, 2007; pp 12−56.
(21) U.S. Patent 6839140 B1, 2002.
(22) Dahlin, A. B.; Tegenfeldt, J. O.; Höök, F. *Anal. Chem.* **2006**, *78*, 4416−4423.
(23) Nie, S.; Emory, S. R. *Science* **1997**, *275*, 1102−1106.
(24) Wong, Y. H.; Thomas, R. L.; Hawkins, G. F. *Appl. Phys. Lett.* **1978**, *32*, 538−539.
(25) Franko, M.; Tran, C. D. *J. Phys. Chem.* **1991**, *95*, 6688−6696.
(26) Tsunoda, K.-I.; Nomura, A.; Yamada, J.; Nishi, S. *Appl. Spectrosc.* **1989**, *43*, 49−55.
(27) O'Keefe, A.; Deacon, D. A. G. *Rev. Sci. Instrum.* **1988**, *59*, 2544−2551.
(28) Hodgkinson, J.; Masiyano, D.; Tatam, R. P. *Appl. Opt.* **2009**, *48*, 5748−5758.
(29) Greener, J.; Abbasi, B.; Kumacheva, E. *Lab Chip* **2010**, *10*, 1561−1566.
(30) Wiersma, D. S.; Bartolini, P.; Lagendijk, A.; Righini, R. *Nature* **1997**, *390*, 671−673.
(31) Schwartz, T.; Bartal, G.; Fishman, S.; Segev, M. *Nature* **2007**, *446*, 52−55.
(32) Gómez Rivas, J.; Sprik, R.; Lagendijk, A.; Noordam, L. D.; Rella, C. W. *Phys. Rev. E* **2001**, *63*, 046613.
(33) Pratesi, F.; Burresi, M.; Riboli, F.; Vynck, K.; Wiersma, D. S. *Opt. Express* **2013**, *21*, A460−A468.
(34) Choi, Y.; Yang, T. D.; Fang-Yen, C.; Kang, P.; Lee, K. J.; Dasari, R. R.; Feld, M. S.; Choi, W. *Phys. Rev. Lett.* **2011**, *107*, 023902.
(35) Svensson, T.; Adolfsson, E.; Lewander, M.; Xu, C. T.; Svanberg, S. *Phys. Rev. Lett.* **2011**, *107*, 143901.
(36) Suarez, G.; Santschi, C.; Dutta-Gupta, S.; Juillerat-Jeanneret, L.; Martin, O. J. F. *Proc. SPIE* **2012**, *8229*, 822908.
(37) Koman, V.; Suárez, G.; Santschi, C.; Cadarso, V. J.; Brugger, J.; von Moos, N.; Slaveykova, V. I.; Martin, O. J. F. *Proc. SPIE* **2013**, *8572*, 857218.
(38) Suarez, G.; Santschi, C.; Slaveykova, V. I.; Martin, O. J. F. *Sci. Rep.* **2013**, *3*, 34471−34478.
(39) Thomas, D.; Maraston, C.; Bender, R.; de Oliveira, C. M. *Astrophys. J.* **2005**, *621*, 673.
(40) Zhang, H. F.; Maslov, K.; Stoica, G.; Wang, L. V. *Nat. Biotechnol.* **2006**, *24*, 848−851.
(41) Matousek, P. *Appl. Spectrosc.* **2006**, *60*, 1341−1347.
(42) Gusak, V.; Heiniger, L.-P.; Zhdanov, V. P.; Gratzel, M.; Kasemo, B.; Langhammer, C. *Energy Environ. Sci.* **2013**, *6*, 3627−3636.
(43) Mujumdar, S.; Torre, R.; Ramachandran, H.; Wiersma, D. *NANOP* **2010**, *4*, 041550.
(44) Uppu, R.; Mujumdar, S. *Opt. Express* **2011**, *19*, 23523−23531.
(45) Berthois, Y.; Katzenellenbogen, J. A.; Katzenellenbogen, B. S. *Proc. Natl. Acad. Sci. U.S.A.* **1986**, *83*, 2496−2500.
(46) Liu, X.; Atwater, M.; Wang, J.; Huo, Q. *Colloids Surf., B* **2007**, *58*, 3−7.
(47) Muskens, O. L.; Bachelier, G.; Fatti, N. D.; Vallée, F.; Brioude, A.; Jiang, X.; Pileni, M.-P. *J. Phys. Chem. C* **2008**, *112*, 8917−8921.
(48) Muskens, O. L.; Billaud, P.; Broyer, M.; Del Fatti, N.; Vallée, F. *Phys. Rev. B* **2008**, *78*, 205410.
(49) Arbouet, A.; Christofilos, D.; Del Fatti, N.; Vallée, F.; Huntzinger, J. R.; Arnaud, L.; Billaud, P.; Broyer, M. *Phys. Rev. Lett.* **2004**, *93*, 127401.
(50) Boyer, D.; Tamarat, P.; Maali, A.; Lounis, B.; Orrit, M. *Science* **2002**, *297*, 1160−1163.
(51) Mitra, A.; Deutsch, B.; Ignatovich, F.; Dykes, C.; Novotny, L. *ACS Nano* **2010**, *4*, 1305−1312.
(52) Chen, W.-Y.; Chen, L.-Y.; Ou, C.-M.; Huang, C.-C.; Wei, S.-C.; Chang, H.-T. *Anal. Chem.* **2013**, *85*, 8834−8840.
(53) Zhang, Y.; Pilapong, C.; Guo, Y.; Ling, Z.; Cespedes, O.; Quirke, P.; Zhou, D. *Anal. Chem.* **2013**, *85*, 9238−9244.
(54) Lee, G. J.; Attri, P.; Choi, E. H.; Kwon, Y.-W.; Krasnikov, I.; Seteikin, A. *J. Nanosci. Nanotechnol.* **2014**, *14*, 221−249.
(55) Davies, K. J. *Biochem. Soc. Symp.* **1995**, *61*, 1−31.
(56) Song, Y.; Driessens, N.; Costa, M.; De Deken, X.; Detours, V.; Corvilain, B.; Maenhaut, C.; Miot, F.; Van Sande, J.; Many, M.-C.; Dumont, J. E. *J. Clin. Endocrinol. Metab.* **2007**, *92*, 3764−3773.
(57) Daniel, W. L.; Han, M. S.; Lee, J.-S.; Mirkin, C. A. *J. Am. Chem. Soc.* **2009**, *131*, 6362−6363.
(58) Kim, A. D. *J. Opt. Soc. Am. A* **2004**, *21*, 820−827.
(59) Muskens, O. L.; Rivas, J. G.; Algra, R. E.; Bakkers, E. P. A. M.; Lagendijk, A. *Nano Lett.* **2008**, *8*, 2638−2642.
(60) Muskens, O. L.; Lagendijk, A. *Opt. Lett.* **2009**, *34*, 395−397.
(61) Uppu, R.; Tiwari, A. K.; Mujumdar, S. *AIP Conf. Proc.* **2011**, *1398*, 103−105.
(62) Henyey, L. G.; Greenstein, J. L. *Astrophys. J.* **1941**, *93*, 70−83.
(63) Liew, S. F.; Forster, J.; Noh, H.; Schreck, C. F.; Saranathan, V.; Lu, X.; Yang, L.; Prum, R. O.; O'Hern, C. S.; Dufresne, E. R.; Cao, H. *Opt. Express* **2011**, *19*, 8208−8217.
(64) Pine, D. J.; Weitz, D. A.; Chaikin, P. M.; Herbolzheimer, E. *Phys. Rev. Lett.* **1988**, *60*, 1134−1137.
(65) Bissonnette, L. R. *Appl. Opt.* **1988**, *27*, 2478−2484.
(66) Mengual, O.; Meunier, G.; Cayré, I.; Puech, K.; Snabre, P. *Talanta* **1999**, *50*, 445−456.
(67) Muskens, O. L.; Diedenhofen, S. L.; Kaas, B. C.; Algra, R. E.; Bakkers, E. P. A. M.; Gómez Rivas, J.; Lagendijk, A. *Nano Lett.* **2009**, *9*, 930−934.
(68) Dullien, F. A. L. *Porous Media. Fluid Transport and Pore Structure*; Academic Press Inc.: San Diego, 1992.
(69) Bohren, C. F.; Huffman, D. R. In *Absorption and Scattering of Light by Small Particles*; Wiley-VCH Verlag GmbH: Berlin, 2007; pp 82−129.

DOI: 10.1021/ac502267q
Anal. Chem. 2015, 87, 1536−1543